Experiment to Detect Dark Energy Forces Using Atom Interferometry

D. O. Sabulsky,* I. Dutta, and E. A. Hinds†
Centre for Cold Matter, Blackett Laboratory, Imperial College London, Prince Consort Road, London SW7 2AZ, United Kingdom

B. Elder, C. Burrage, and Edmund J. Copeland
School of Physics and Astronomy, University of Nottingham, Nottingham NG7 2RD, United Kingdom

(Received 11 February 2019; revised manuscript received 7 June 2019; published 6 August 2019)

The accelerated expansion of the universe motivates a wide class of scalar field theories that modify general relativity (GR) on large scales. Such theories require a screening mechanism to suppress the new force in regions where the weak field limit of GR has been experimentally tested. We have used atom interferometry to measure the acceleration of an atom toward a macroscopic test mass inside a high vacuum chamber, where new forces can be unscreened. Our measurement shows no evidence of new forces, a result that places stringent bounds on chameleon and symmetron theories of modified gravity.

DOI: 10.1103/PhysRevLett.123.061102

The accelerating expansion of the Universe suggests that most of the energy in the Universe is "dark" [1]. One potential explanation is that Einstein gravity receives $O(1)$ corrections from new degrees of freedom. However, the measured success of the weak field limit of GR within the Solar System requires that these corrections be screened in that regime. Two suitably screened fields are the chameleon [2] and the symmetron [3], which couple both to themselves and to matter. Although these theories cannot drive accelerated expansion without vacuum energy [4], they remain interesting as a way to hide modifications to Einstein gravity.

We proposed [5] that such forces might be detected by using atom interferometry to measure the attraction of an atom in ultrahigh vacuum toward a macroscopic test mass. This is an ideal technique because atoms are sufficiently small that they are unscreened probes of the fifth force. Our proposal was pursued by Hamilton *et al.* [6–8]. Here we report an independent atom interferometry measurement, using a significantly different experimental method, which achieves very similar sensitivity and confirms that a large part of the parameter space is now excluded.

Figure 1 illustrates the principle of the experiment. The walls of the stainless steel vacuum chamber are at $\pm Z$, where their high density drives the chameleon or symmetron field ϕ to a low value. Inside the empty chamber ϕ rises to a maximum, ϕ_{bg}, illustrated by the red curve. A metal ball placed in the vacuum at position 1 forces a dip in ϕ_{bg} (dashed blue line), creating a gradient of ϕ near the ball. An atom at the center of the chamber is accelerated by this gradient toward the ball, with acceleration a_ϕ. We use atom interferometry to measure the component of a_ϕ along the axis marked $\pm Z$. When the ball is moved to position 2 (dotted blue line), this component of a_ϕ reverses, and we look for the change of acceleration.

Atom interferometry with stimulated Raman transitions [9,10] is a sensitive technique for detecting small accelerations. It is well established as the basis for ultrasensitive gravimeters [11], gyroscopes [12], magnetometers [13], and accelerometers [14] and for applications in metrology [15,16], tests of general relativity [17], and gravitational wave detection [18–20].

Figure 2 illustrates our experiment, in which counterpropagating laser beams along the z axis, differing in frequency by 6.8 GHz, drive the clock transition in rubidium-87 atoms through a Raman process. At time $t = 0$ a $\pi/2$

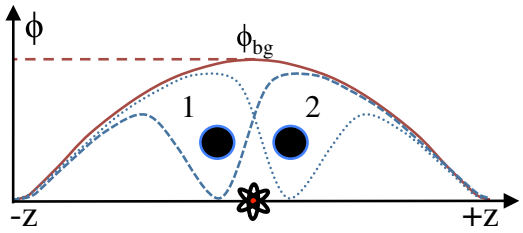

FIG. 1. Principle of the experiment [5]. Vacuum chamber walls are at $\pm Z$. Solid red curve: scalar field ϕ is small at $\pm Z$, rising to ϕ_{bg} at the center of the empty chamber. Dashed(dotted) blue curve: ball in position 1(2) perturbs ϕ to produce a gradient $\nabla\phi$. Atoms at the center of the chamber have acceleration $a_\phi \propto \nabla\phi$ toward the ball, which we measure by atom interferometry.

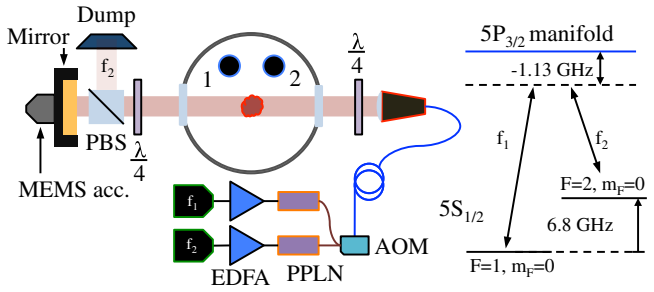

FIG. 2. Laser beams of frequency f_1 and f_2 are coupled into two crossed linear polarizations of a polarization-maintaining optical fiber. The fiber output is expanded and collimated to form a beam of 20.9 mm radius (e^{-2} intensity), which passes though a quarter-wave plate to make the two frequency components oppositely circularly polarized. A second quarter-wave plate restores the linear polarization so that a polarizing beam splitter can dump the f_2 beam, while a mirror retro-reflects the f_1 beam. At the atom cloud, the counterpropagating f_1 and f_2 beams have the same circular polarization, as required to drive the ^{87}Rb clock transition, as indicated on the right.

pulse creates a superposition of the two clock states, which move apart because of the photon recoil momentum. After time T, a π pulse swaps the two internal states and reverses the recoil velocity so that the two parts of the wave function overlap at time $t = 2T$. A final $\pi/2$ pulse closes the interferometer to give $\cos^2(\varphi/2)$ and $\sin^2(\varphi/2)$ fringes in the populations of the two clock states, where φ is the quantum mechanical phase difference accumulated along the two paths. We determine φ by measuring the final populations in the clock states, and φ is proportional to the acceleration of the atoms along the direction of the laser beams. To constrain scalar forces we look for a change in φ when the ball is moved.

Inside the vacuum chamber, the density of residual gas is dominated by 9.6×10^{-10} mbar of H_2. The ball is a 19-mm-radius aluminum sphere, coated with Alion MH2200 paint to minimize the scattering of laser beams. This is suspended from a 6-mm-thick aluminium rod, eccentrically mounted on a rotary vacuum feedthrough, which allows the position of the ball to be changed, as in Fig. 2. A 2D magneto-optical trap (MOT) [21] injects a pulse of cold ^{87}Rb atoms into the chamber through a differential pumping hole. A 3D MOT [22] collects $\sim 10^8$ atoms at the center of the chamber, then optical molasses cools them to 5 μK before the cooling light is switched off, followed by the repump light once it has pumped all the atoms into the $5S_{1/2}(F = 2)$ states.

We use Raman transitions to initialize and operate the atom interferometer. The light is delivered to the atoms as shown in Fig. 2. Lasers of frequency f_1 and f_2 are phase locked to make a beat note, detuned by Δf from the 6.8 GHz clock transition $|F = 2, M_F = 0\rangle \rightarrow |F = 1, M_F = 0\rangle$, which is resolved from the other hyperfine transitions by the Zeeman shifts in a 1.7 G magnetic field. The resonance frequency is Doppler shifted by the atom's velocity component $v_\parallel$ along the Raman beams. With a detuning of $\Delta f = -72$ kHz and a pulse length of 4.5 μs, atoms in the velocity range $v_\parallel = 30 \pm 23$ mm/s are driven to the state $|F = 1, M_F = 0\rangle$, after which we remove the remaining $F = 2$ atoms using resonant light pressure.

This state-selected, velocity-selected group of $N_0 \simeq 10^6$ atoms is then subjected to three interferometer pulses, spaced by time intervals $T = 16$ ms and having pulse areas of $\pi/2$, π, and $\pi/2$, respectively [9]. After the third pulse, the fraction of atoms in state $|F = 2, M_F = 0\rangle$ is

$$\mathcal{P} = \frac{1}{2}(1 - \eta\cos(\varphi + \varphi_0)), \tag{1}$$

where

$$\varphi = \frac{2\pi(f_1 + f_2)}{c} T^2 \mathbf{n} \cdot \mathbf{a}, \tag{2}$$

and $\mathbf{n} \cdot \mathbf{a}$ is the acceleration of the atoms relative to the mirror, projected onto the mirror normal $\mathbf{n}$. The fringe visibility η depends on the inhomogeneous width of the Raman transition, which depends on the range of velocities selected. The angle φ_0 in Eq. (1) is a phase shift applied to the last Raman pulse, which we switch between 0 and π on alternate shots of the experiment. The difference in $\mathcal{P}$ for these two phases is $\Delta\mathcal{P} = \eta\cos\varphi$. Each interferometer sequence ends with a measurement of $\mathcal{P}$ using laser-induced fluorescence. Measurements alternate between $\varphi_0 = 0$ and π to determine $\Delta\mathcal{P}$, and hence φ.

In total, $\mathbf{n} \cdot \mathbf{a}$ in Eq. (2) comprises three parts:

$$\mathbf{n} \cdot \mathbf{a} = \mathbf{n} \cdot (\mathbf{a}_{\text{ball}} + \mathbf{g} + \mathbf{a}_{\text{noise}}). \tag{3}$$

The term $\mathbf{a}_{\text{ball}}$ includes the Newtonian attraction and the anomalous acceleration $\mathbf{a}_\phi$ towards the ball. The second term represents the ambient gravitational field. The last term is the acceleration noise of the mirror, due mainly to acoustic vibrations. In order to distinguish the first term from the other two, we mount a navigation grade FLEX accelerometer (Honeywell, QA750) on the back of the mirror, and plot the $\Delta\mathcal{P}$ fringes against the voltage V_M registered by that accelerometer, as shown in Fig. 3(a). The phase of the fringe pattern only senses changes in $\mathbf{n} \cdot \mathbf{a}_{\text{ball}}$, because the atomic and FLEX accelerometers both experience the same $\mathbf{n} \cdot (\mathbf{g} + \mathbf{a}_{\text{noise}})$ [23,24], whereas the FLEX accelerometer, being far from the ball, does not register $\mathbf{n} \cdot \mathbf{a}_{\text{ball}}$. Zero offset in the FLEX accelerometer is avoided by alternating the position of the source mass between positions 1 and 2, flipping the sign of $\mathbf{n} \cdot \mathbf{a}_{\text{ball}}$ [25]. The data points in Fig. 3(a) show a typical 12-h set of fringes in $\Delta\mathcal{P}$ obtained by tilting the experiment to scan $\mathbf{n} \cdot \mathbf{g}$, and hence φ. The total change of angle from one end of Fig. 3 to the other is ~ 350 μrad. The red(blue) points are measured with

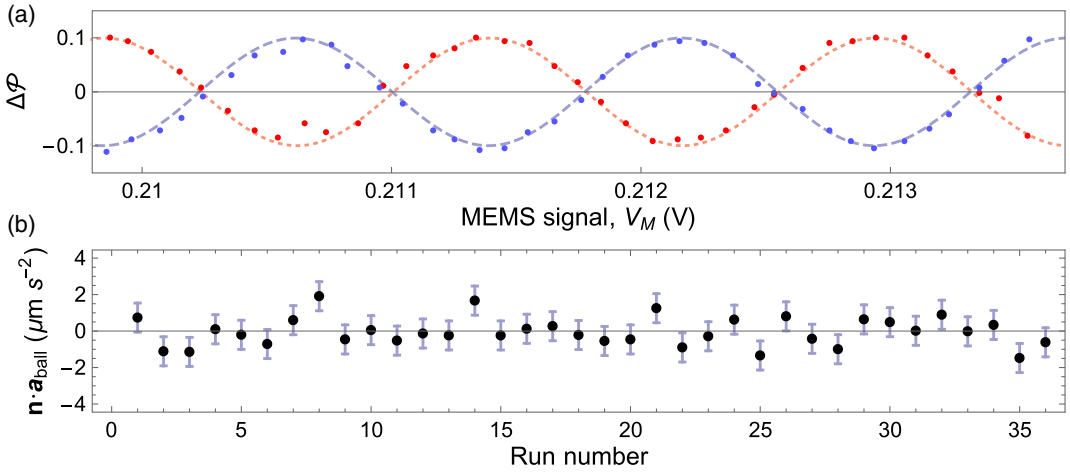

FIG. 3. Experimental data. (a) Typical 12-h run to measure $\Delta\mathcal{P}$ as a function of the voltage recorded by the FLEX accelerometer. This is scanned by tipping the table on which the atom accelerometer sits. Red points: ball in position 1. Here 5774 shots of the interferometer gave 2887 measurements of $\Delta\mathcal{P}$, averaged in bins of 100 μV width. Blue points: ball in position 2, data inverted for clarity. Dashed lines: fits to $\Delta\mathcal{P} = \eta\cos\varphi$. (b) Our 36 independent measurements of $\mathbf{n}\cdot\mathbf{a}_{\rm ball}$. Error bars indicate the standard deviation of these points.

the ball in position 1(2). We fit these to $\eta\cos(\alpha V_M + \theta_{1(2)})$, where α converts FLEX voltage to interferometer phase, and $\theta_{1(2)}$ is the phase offset due to $\mathbf{n}\cdot\mathbf{a}_{\rm ball}$.

Figure 3(b) plots 36 values of $\mathbf{n}\cdot a_{\rm ball}$ derived from our measurements of $\theta_1 - \theta_2$ in November 2017, which average to -42 ± 133 nm/s^2. Taking the force to be toward the center of the ball (at 48.8° to the mirror normal $\mathbf{n}$), we find a repulsive acceleration $a_{\rm ball} = -64 \pm 201$ nm/s^2. This includes contributions from the Newtonian attraction and potentially magnetic and electric field gradients, summarized in Table I.

With a center-to-center spacing of 26.8 mm, as close as possible without scattering Raman light, the Newtonian acceleration is 7.2 nm/s^2. Movement of the atoms through a small magnetic field gradient produces a false acceleration towards the ball of $+6 \pm 5$ nm/s^2 [26] due to the Zeeman shift of the clock transition. The electric analog of this is negligible because the Stark shift of the clock transition involves the very small tensor polarizability. Instead, an electric field gradient can produce a real acceleration of the atoms through their scalar polarizability. The ball was grounded to the chamber, but may have been electrically charged because aluminium naturally grows a surface layer of alumina ~4 nm thick and can support a potential difference of up to ~1 V before breaking down. Assuming that the surface is indeed charged to ≤ 1 V, this effect contributes $\leq +1.5$ nm/s^2. Ultimately, we determine

$$a_\phi = -77 \pm 201 \text{ nm s}^{-2}, \tag{4}$$

where the uncertainty is almost entirely due to statistical noise. We conclude with 90% confidence that $a_\phi < +183$ nm/s^2.

TABLE I. Systematic corrections to $a_{\rm ball}$.

	Value (nm s^{-2})
Measured $a_{\rm ball}$	-64 ± 201
Newtonian gravity	$+7$
Magnetic field gradients	$+6 \pm 5$
Electric field gradients	$< +2$
Final value for a_ϕ	-77 ± 201

Key experimental differences between this work and that of Ref. [8] are our interferometry used freely propagating laser light, not light in a cavity; we measured the force horizontally, not against a large background due to gravity (requiring a chirped interferometer); we used a spherical, aluminum test mass not a cylindrical, tungsten one; we used Rb instead of Cs atoms. For chameleon and symmetron models, these differences in the source and test bodies change where in the parameter space the fifth force is screened. More generally, these differences may be significant if the force is sensitive, for example, to the density of the source or to the nuclear composition of the masses.

This bound on a_ϕ places an upper limit on the strength of screened fifth forces. The general action is (with the mostly plus metric signature)

$$S_\phi = \int d^4x\sqrt{-g}\left(-\frac{1}{2}(\partial\phi)^2 - V(\phi) - A(\phi)\rho_{\rm m}\right), \tag{5}$$

where $\rho_{\rm m}$ is the density of nonrelativistic matter. The equation of motion for ϕ is

$$\vec{\nabla}^2\phi = \frac{dV}{d\phi} + \frac{dA}{d\phi}\rho_{\rm m}. \tag{6}$$

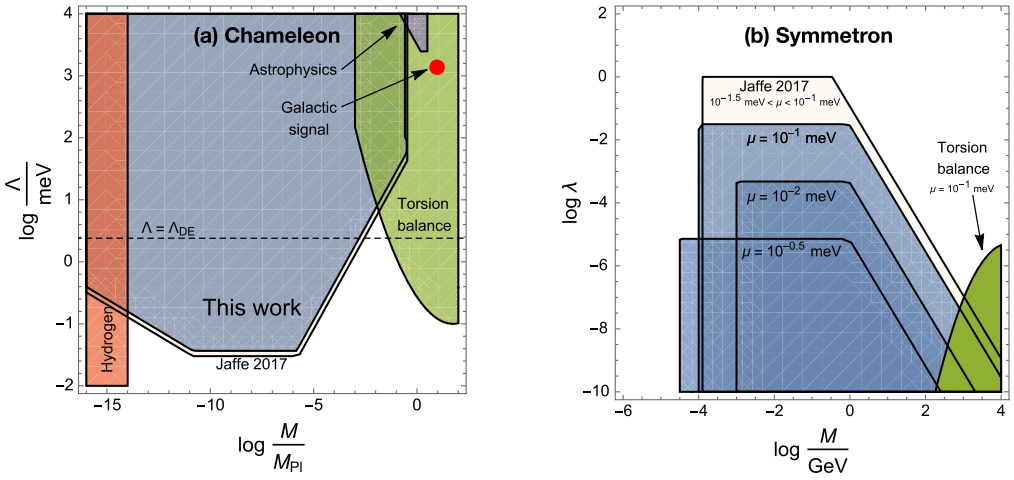

FIG. 4. Constraints on chameleon and symmetron parameters; shaded regions are excluded. The black line on (a) marks the dark energy scale $\Lambda = \sqrt{3 M_{\rm Pl} H_0} \sim$ meV, where H_0 is the Hubble constant [32]. The red dot indicates the values of the chameleon parameters consistent with the astrophysical signal of [33,34]. For the symmetron (b), only a range of approximately 1.5 orders of magnitude in μ is probed, as is typical of laboratory tests. The galactic signal would correspond to a very different region, $\mu \sim 10^{-26}$ meV. Current bounds may be found in [35–39].

The acceleration of a small, freely falling extended object due to ϕ is [27]

$$\vec{a}_\phi = \lambda_{\rm a} \frac{dA}{d\phi} \vec{\nabla}\phi(\vec{x}). \tag{7}$$

The screening factor λ_a varies between 0 for large and dense (*screened*) objects and 1 for small and light (*unscreened*) objects.

The prototypical chameleon field has a self-interaction potential $V(\phi) = \Lambda^5/\phi$ and matter coupling $A(\phi) = \phi/M$ and the screening factor for a spherical object of radius $R_{\rm obj}$ and density $\rho_{\rm obj}$ is approximately $\lambda_{a,\rm cham} \approx \min[(3M\phi_{\rm env})/(\rho_{\rm obj} R_{\rm obj}^2), 1]$, where $\phi_{\rm env}$ is the ambient field value.

We solve Eq. (6), where $\rho_{\rm m}$ includes the source mass, vacuum chamber gas, and walls. A general solution is unknown; however, it may be solved exactly for an infinite plate. It may also be solved numerically.

The distance $x = 0.775$ cm from the atoms to the surface of the sphere is less than half the radius of the sphere, so we approximate the sphere as an infinite plate [28,29]. The plate is assumed to be sufficiently dense that $\phi \approx 0$ at the surface. We include a geometrical fitting factor ξ, which is determined numerically.

The chameleon field is approximated as [28,30,31]

$$\phi_{\rm cham} = \xi_{\rm cham} (9\Lambda^5/2)^{1/3} x^{2/3}. \tag{8}$$

We determine $\xi_{\rm cham}$ by solving Eq. (6) on a 3-dimensional grid [7,8], with $\phi = 0$ at the surfaces of the vacuum chamber and sphere, and negligible gas density. When these approximations are not appropriate (for chameleon parameter $M \lesssim 10^{-10} M_{\rm Pl}$ and $M \gtrsim 10^{-0.5} M_{\rm Pl}$ with $M_{\rm Pl}$ the reduced Planck mass), we use an analysis identical to that of [5,6].

Comparing our numerical results with Eq. (8), we find $\xi_{\rm cham} = 1.11$ for 10^{-5} eV $< \Lambda < 10^5$ eV. This insensitivity of $\xi_{\rm cham}$ to Λ is guaranteed by the vacuum scaling symmetry $\phi \to a\phi, \Lambda \to a^{3/5}\Lambda$. Equation (7) may now be used to compute the chameleon force on a rubidium-87 nucleus. The constraints are plotted in Fig. 4(a).

The symmetron has a potential $V(\phi) = -\frac{1}{2}\mu^2\phi^2 + (\lambda/4)\phi^4$ and coupling $A(\phi) = \phi^2/2M^2$, and the screening factor for a spherical object is [3] $\lambda_{a,\rm symm} \approx \min[(M^2/\rho_{\rm obj} R_{\rm obj}^2), 1]$. When the ambient matter density $\rho_{\rm m}$ is small, the field reaches $\phi \approx \mu/\sqrt{\lambda}$ at the minimum of its effective potential $V_{\rm eff} = V + A\rho$. If $\rho_{\rm m} > \mu^2 M^2$, the minimum of the effective potential is $\phi = 0$. The scalar force Eq. (7) is proportional to the local field value, so large ambient matter densities shut off the scalar force.

The experiment tests the window 10^{-2} meV $< \mu \lesssim 10^{-1}$ meV. The upper bound is due to the force becoming short ranged, while at the lower bound it is so long ranged that $\phi = 0$ everywhere inside the vacuum chamber [29]. The approximate solution to the symmetron field near the atoms is a product of a fitting factor $\xi_{\rm symm}$ and the 1D solution [29,40,41]

$$\phi_{\rm symm} = \xi_{\rm symm} (\mu/\sqrt{\lambda}) \tanh(\mu x/\sqrt{2}). \tag{9}$$

The symmetron equation of motion in vacuum also admits a scaling symmetry $\phi \to a\phi$, $\lambda \to (1/a^2)\lambda$, which guarantees that $\xi_{\rm symm}$ is independent of λ. A similar argument does not apply for μ. We have numerically solved the equation of motion for 10^{-2} meV $< \mu <$ 300 meV, and

found that $1 < \xi_{\mathrm{symm}} < 1.5$. We conservatively set $\xi_{\mathrm{symm}} = 1$. Our constraints, illustrated in Fig. 4(b), cover a similar but slightly wider range of μ than those of [8].

There exist strong bounds from bouncing neutrons but, under standard assumptions about screening, those results [Fig. 4(b) of [39]] constrain a different window of μ. The two experimental methods are therefore complementary. Recently Refs. [33,34] have reported the detection of a signal, at 6–7σ, consistent with screened fifth forces on Mpc scales. Those studies use a somewhat schematic screening model that, when interpreted as a chameleon model, corresponds to the point indicated with a red dot in Fig. 4, in tension with existing torsion balance constraints. Interpreted as a symmetron model, this galactic signal corresponds to $\mu \sim 10^{-26}$ meV, many orders of magnitude away from the range, presented in Fig. 4, that is accessible in the laboratory.

In conclusion, we have measured the acceleration of ^{87}Rb atoms toward a test mass in a high-vacuum environment. We find no evidence for screened fifth forces, which now seem to be ruled out by two independent tests over a wide range of the parameter space of prototypical chameleon and symmetron models. There remains a key region of parameter space available to chameleon models with $\Lambda \sim \Lambda_{\mathrm{DE}}$, and much unconstrained parameter space for the symmetron model. We believe that this gap can be closed by an upgrade, in progress, to our experiment that will lower the noise floor to the quantum projection limit.

We acknowledge engineering support by J. Dyne, S. Maine, G. Marinaro, and V. Gerulis and financial support by EPSRC, Dstl, the Royal Society, the Leverhulme Trust (C. B. and B. E.), and STFC Grant No. ST/P000703/1 (E. J. C.). D. O. S. acknowledges the Marie Skłodowska Curie Early Stage Researcher program and Action-Initial Training Network FP7/2007-2013.

*Present address: Laboratoire Photonique, Numérique et Nanosciences, Université Bordeaux-IOGS-CNRS:UMR 5298, rue F. Mitterrand, F-33400 Talence, France.
†ed.hinds@imperial.ac.uk

[1] E. J. Copeland, M. Sami, and S. Tsujikawa, Int. J. Mod. Phys. D **15**, 1753 (2006).
[2] J. Khoury and A. Weltman, Phys. Rev. D **69**, 044026 (2004).
[3] K. Hinterbichler and J. Khoury, Phys. Rev. Lett. **104**, 231301 (2010).
[4] J. Wang, L. Hui, and J. Khoury, Phys. Rev. Lett. **109**, 241301 (2012).
[5] C. Burrage, E. J. Copeland, and E. A. Hinds, J. Cosmol. Astropart. Phys. 03 (2015) 042.
[6] P. Hamilton, M. Jaffe, P. Haslinger, Q. Simmons, H. Müller, and J. Khoury, Science **349**, 849 (2015).
[7] B. Elder, J. Khoury, P. Haslinger, M. Jaffe, H. Müller, and P. Hamilton, Phys. Rev. D **94**, 044051 (2016).
[8] M. Jaffe, P. Haslinger, V. Xu, P. Hamilton, A. Upadhye, B. Elder, J. Khoury, and H. Müller, Nat. Phys. **13**, 938 (2017).
[9] M. A. Kasevich and S. Chu, Phys. Rev. Lett. **67**, 181 (1991).
[10] A. Peters, K. Y. Chung, and S. Chu, Nature (London) **400**, 849 (1999).
[11] Q. Bodart, S. Merlet, N. Malossi, F. P. D. Santos, P. Bouyer, and A. Landragin, Appl. Phys. Lett. **96**, 134101 (2010).
[12] I. Dutta, D. Savoie, B. Fang, B. Venon, C. L. Garrido Alzar, R. Geiger, and A. Landragin, Phys. Rev. Lett. **116**, 183003 (2016).
[13] D. A. Braje, S. A. Desavage, C. L. Adler, J. P. Davis, and F. A. Narducci, J. Mod. Opt. **61**, 61 (2014).
[14] R. Geiger, V. Ménoret, G. Stern, N. Zahzam, P. Cheinet, B. Battelier, A. Villing, F. Moron, M. Lours, Y. Bidel, A. Bresson, A. Landragin, and P. Bouyer, Nat. Commun. **2**, 474 (2011).
[15] D. S. Weiss, B. C. Young, and S. Chu, Phys. Rev. Lett. **70**, 2706 (1993).
[16] R. Bouchendira, P. Cladé, S. Guellati-Khélifa, F. Nez, and F. Biraben, Phys. Rev. Lett. **106**, 080801 (2011).
[17] S. Dimopoulos, P. W. Graham, J. M. Hogan, and M. A. Kasevich, Phys. Rev. Lett. **98**, 111102 (2007).
[18] S. Dimopoulos, P. W. Graham, J. M. Hogan, M. A. Kasevich, and S. Rajendran, Phys. Lett. B **678**, 37 (2009).
[19] W. Chaibi, R. Geiger, B. Canuel, A.Bertoldi, A. Landragin, and P. Bouyer, Phys. Rev. D **93**, 021101(R) (2016).
[20] B. Canuel *et al.*, Sci. Rep. **8**, 14064 (2018).
[21] K. Dieckmann, R. J. C. Spreeuw, M. Weidemüller, and J. T. M. Walraven, Phys. Rev. A **58**, 3891 (1998).
[22] K. Lindquist, M. Stephens, and C. Wieman, Phys. Rev. A **46**, 4082 (1992).
[23] The FLEX accelerometer measures along the normal to the mirror. Although **g** is slightly different for the atoms and the accelerometer, the difference is small enough to neglect.
[24] S. Merlet, J. LeGouët, Q. Bodart, A. Clairon, A. Landragin, F. Pereira Dos Santos, and P. Rouchon, Metrologia **46**, 87 (2009).
[25] This does tilt the table, changing $\mathbf{n} \cdot \mathbf{g}$ by 125.4(1) nm/s^2, but that affects the atoms and the FLEX accelerometer equally so it does not shift φ.
[26] D. Sabulsky, Ph.D. thesis, Imperial College, London, 2018.
[27] L. Hui, A. Nicolis, and C. W. Stubbs, Phys. Rev. D **80**, 104002 (2009).
[28] A. Upadhye, Phys. Rev. D **86**, 102003 (2012).
[29] A. Upadhye, Phys. Rev. Lett. **110**, 031301 (2013).
[30] C. Burrage, E. J. Copeland, and J. A. Stevenson, J. Cosmol. Astropart. Phys. 08 (2016) 070.
[31] A. N. Ivanov, G. Cronenberg, R. Höllwieser, T. Jenke, M. Pitschmann, M. Wellenzohn, and H. Abele, Phys. Rev. D **94**, 085005 (2016).
[32] N. Aghanim *et al.* (Planck Collaboration), arXiv:1807.06209.
[33] H. Desmond, P. G. Ferreira, G. Lavaux, and J. Jasche, Phys. Rev. D **98**, 083010 (2018).
[34] H. Desmond, P. G. Ferreira, G. Lavaux, and J. Jasche, Phys. Rev. D **98**, 064015 (2018).
[35] P. Brax and A.-C. Davis, Phys. Rev. D **94**, 104069 (2016).

[36] C. Burrage and J. Sakstein, Living Rev. Relativity **21**, 1 (2018).
[37] P. Brax, A.-C. Davis, B. Elder, and L. K. Wong, Phys. Rev. D **97**, 084050 (2018).
[38] P. Brax and S. Fichet, Phys. Rev. D **99**, 104049 (2019).
[39] G. Cronenberg, P. Brax, H. Filter, P. Geltenbort, T. Jenke, G. Pignol, M. Pitschmann, M. Thalhammer, and H. Abele, Nat. Phys. **14**, 1022 (2018).
[40] P. Brax and M. Pitschmann, Phys. Rev. D **97**, 064015 (2018).
[41] C. Burrage, B. Elder, and P. Millington, Phys. Rev. D **99**, 024045 (2019).